Chem Rev Lett 8 (2025) 112-127

Research Article

Chemical Review and Letters
journal homepage: www.chemrevlett.com
ISSN (online): 2645-4947 (print) 2676-7279

Zeolitic-imidazolate framework synthesized with the mechanochemical method: impressive removal of nine reactive dyes of wastewaters

Shabnam Alibakhshi [1, 2], Ashraf S. Shahvelayati[1, 2, *], Maryam Ranjbar[3]

[1]*Department of Chemistry, College of Basic Sciences, Yadegar-e- Imam Khomeini (RAH) Shahre Ray Branch, Islamic Azad University, Tehran, Iran*
[2]*Research Center for New Technologies in Chemistry and Related Sciences, Yadegar-e-Imam Khomeini (RAH) Shahre Rey Branch, Islamic Azad University, Tehran, Iran*
[3]*Department of Chemical Technologies, Iranian Research Organization for Science and Technology (IROST), Tehran, Iran*

ARTICLE INFO

Article history:
Received 12 November 2024
Received in revised form 11 December 2024
Accepted 13 December 2024
Available online 15 January 2025

Keywords:
Zeolitic-imidazole framework,
dye adsorption, wastewaters,
isotherm models, kinetic studies

ABSTRACT

The effective elimination of dyes from the aquatic environment is one of the serious environmental goals. Herein we describe the synthesis (by the Mechanochemical Method), and application of a catalyst zeolitic-imidazolate framework (ZIF-8) for the impressive removal of various types of dyes such as Remazol golden yellow RNL(RD_1), Blue94 (RD_2), Red141(RD_3), Violet-5r (RD_4), Red66 (RD_5), Red195 (RD_6), Red120 (RD_7), Yellow160 (RD_8), Yellow176 (RD_9) in the wastewaters through the adsorption process. The effects of temperature, pH, dye concentration, contact time, and adsorption dose on the adsorption process were investigated and optimized. The isotherm models were studied through four-parameter equations, Freundlich, Langmuir, Tepmkin, and Dubinin-Radushkevich. The adsorption isotherm data showed the Langmuir model was the consistent model. The COD and BOD in the real sample were determined in the presence of the catalyst, and results show the values of BOD and COD were significantly reduced. The structure of the synthesized catalyst was characterized by various techniques including FTIR, SEM, XRD, specific surface area, and BET. The high adsorption capacity, reusability, and recyclability of the catalyst were some of the advantages of the prepared catalyst.
This catalyst was utilized as an efficient adsorbent for the removal of dyes from textile wastewater. The observed results show a significant reduction in BOD and COD using the prepared catalyst.

1. Introduction

Nowadays, the elimination of environmental pollutants has been a hot topic for scientists. Discharging the colored wastewater of the textile industry in the environment because of high toxicity, is one of the serious environmental challenges and created many environmental and health problems [1]. Azo-reactive dyes are one of the major pollutants that cannot be removed from the environment by current conventional methods. Reactive azo dyes have extensive use in textile industries and provide many dyes discharged into the environment [2, 3]. Moreover, reactive dyes have resistance to natural biodegradation owing to the aromatic rings in their structure [4]. It is a potential danger to the aquatic environment owing to its poor biodegradability [5]. "Photocatalytic degradation using nanocatalysts and adsorption are two essential methods for dye removal [6, 7]. The toxicity of nanocatalysts remains a challenging issue.
Recently, the development of catalyst/chitosan or zeolite composites has gained attention as a promising approach to mitigate the potential risks associated with catalyst toxicity while preserving catalytic efficiency [8-11].

∗ Corresponding authors; e-mail: avelayati@yahoo.com
https://doi.org/10.22034/crl.2024.483081.1448

Adsorption is regarded as the identity of the most effective, attractive, and simple method. Numerous materials have been used as adsorbents, including porous silica, activated carbon, zeolites, and porous polymers [12-18]. Hence, it is still vital to establish robust and effective capacity adsorbents. Metal-organic frameworks (MOFs) display a significant difference in potential reinforcements [19, 20], such as, gas storage [21, 22], gas separation [23], catalysis [24, 25], energy storage [26, 27] and biomedical applications [28, 29]. MOFs-based materials obtained numerous applications for the removal and adsorption of pollutants in recent years [30-32]. The ZIF-8 [Zn (2-methylimidazole) $_2.2H_2O$] formed from 2-methyl imidazole ligands and Zn (II) center ions dispense more excellent chemical and thermal resistance than other MOFs [33], and nano-sized of ZIF-8 is more beneficial for removing reactive dyes.

The strategies for the synthesis of ZIF-8 nanocrystals are still challenging. Presently, the solvothermal outline in polar solvents such as *N*, *N*-dimethyl formamide, or methanol, seems applied intensively since its significant advantages were proven as high-yield and simple processes [34]. In this work, the ZIF-8 crystals from Zn $(NO_3)_2{\cdot}6H_2O$ and 2-HMim ligand were rapidly synthesized under ultrasonic conditions and sonochemical method in high yield. Response surface methodology method can be applied to optimize the experimental parameters to remove models of reactive dyes (RD_1), (RD_2), (RD_3), (RD_4), (RD_5), (RD_6), (RD_7), (RD_8), and (RD_9). The Langmuir, Freundlich, Temkin, and Dubinin–Radushk-evich (D–R) isotherm models assessed the adsorption equilibrium. A kinetic study was also performed using pseudo-first-order, pseudo-second-order, first-order reaction model, second-order reaction model, intraparticle diffusion, and Elovich models. Furthermore, thermodynamic parameters were also evaluated by Van't Hoff equation. Finally, the adsorption mechanism of reactive dyes on the surface of ZIF-8 was adequately discussed.

2. Material and Methods

All chemicals adopted in this work were purchased from Sigma-Aldrich and utilized as received without extra purification. The dyes Remazol Golden Yellow RNL (RD_1), Red 195 (RD_6), Red 120 (RD_7), Everzol Yellow 3RS/HC, Yellow 176 (RD_9), RY 160 (RD_8), Red 141 (RD_3), Remazol Brilliant Violet (RB-5R) (RD_4), Blue 94 (RD_2), and Red 66 (RD_5) (Fig. S1) were purchased from, D.Z.E dye company (Number: 3310350). The natural textile waster water, including orange and red Bemacron SER-DL, was collected from the Farizad textile Dying Factory in Varamin, Iran. The crystalline nature of ZIF-8 was analyzed by X-ray powder diffraction (XRD) pattern, (model X'Pert PRO MPD, PANalytical, Made in the Netherland). Fourier transform-infrared (FT-IR) spectra were recorded on KBr pellets with a Tensor 27 Bruker spectrophotometer. To the concentration of the dye, a double beam UV-visible spectrophotometer was used (Cary 60, Agilent Technologies, and the USA). To estimate the *pH* of solutions, a *pH*-meter was used (S47-K seven Multi, Mettler-Toledo, and Columbus, OH, USA). The ultrasound-aided synthesis process was performed through an ultrasonic bath. Brunauer-Emmett-Teller (BET) surface area measurements and pore volumes were performed by Belsorp mini II Bel (Japan). The ball mill apparatuses Retsch Model PM 100 with zirconia balls have been used. The concentration level of remaining COD and BOD in the real sample was determined by the standard methods, using USA-HACH spectrophotometer and Lutron DO meter. The morophologies and elemental analysis were assessed by a scanning electron microscope SEM (Mira lll, Tescan, Czech Republic) supplied with energy dispersive X-ray analysis (EDAX).

3. Preparation of ZIF-8

Based on the literature, the ZIF-8(A) was prepared through three approaches.

I) The solvothermal method [35]: 3.74 g of Zn $(NO_3)_2.6H_2O$ (11.66 mmol) and 0.83 g of 2-methylimidazol (12.64 mmol) were dissolved in 45 mL DMF, and put in a Teflon line autoclave at 140 ℃ for 24 h. After removing the solvent, the residue was centrifuged and washed with 15 mL chloroform. The colorless polyhedral crystals.

product was dried under vacuum at 200 ℃ for 6 h (yield: 1 g, 67.18%) (**Fig. 1a**).

II) The ultrasonic-assisted solvothermal method. The mixture of Zn $(NO_3)_2.6H_2O$ (3.74 g, 11.66 mmol), and 2-methylimidazole (1.2 g, 12.64 mmol) was dissolved in 45 mL of DMF under ultrasonic conditions. After 30 min, the solution was placed in a stainless autoclave and heated at 140 ℃ for 24 h. After removing the solvent, the residue was collected by centrifuging and washed with chloroform (15 mL). Colorless polyhedral crystals were placed under a vacuum at 200 ℃ for 6 h. The yield was 1.2 g, 80.62 % (**Fig. 1b**).

III) The mechanochemical treatment was performed with in a ball mill [36]: Zn $(NO_3)_2.6H_2O$ (3.74 g, 11.66 mmol) and 2-methylimidazole (0.83 g, 12.64 mmol) as solid form were placed in ball mill (4000 cycle/sec) for 3 h. The yield was 1.4 g, 98.76 % (**Fig. 1c**).

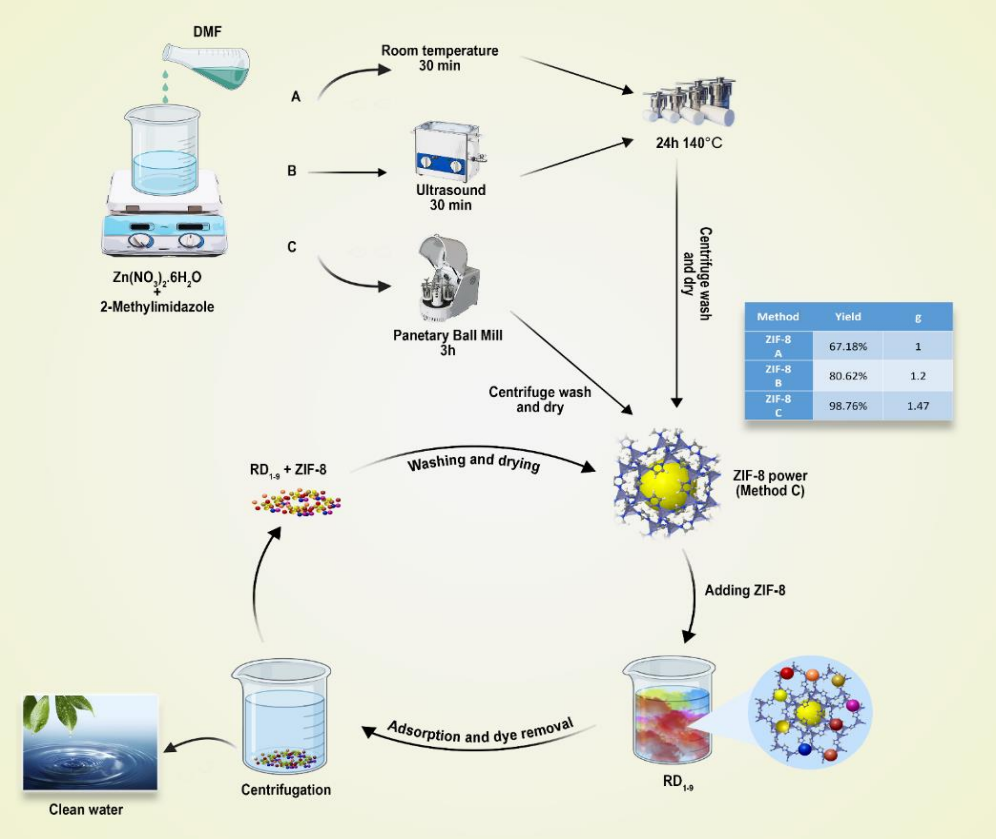

Fig. 1. The preparation of ZIF-8(C) by: (A) The solvothermal method, (B) The ultrasonic-assisted solvothermal method, (C) The mechanochemical treatment in a ball mill

4. Adsorption study

Dye removal experiment an aqueous solution with variable concentrations of reactive dyes was utilized as simulated wastewater to examine the adsorption characteristic of ZIF-8(C) composites. Dissolving the reactive dye in deionized water, it was then diluted to the required concentration. Then, the changes in the absorbance of all solution samples were detected and determined during the adsorption method. Here, nine different types of organic and reactive dyes such as: (RD_1), (RD_2), (RD_3), (RD_4), (RD_5), (RD_6), (RD_7), (RD_8), and (RD_9) were considered for adsorption and removal studies.

At first, 1000 mg\L aqueous solutions of each dye were made beforehand, while adsorption, dye solution at several concentrations were achieved by the progressive dilution of the abovementioned stock solutions. ZIF-8(C) compounds (0.002-0.01 g) were added typically to the dye solutions (10-400 mg/L) and observed by UV-vis absorption spectroscopy at the calibrated maximum wavelengths (I = 411,593, 493, 560, 510, 543, 535,426 and 411 nm, consistent to abovementioned dyes in sequence).

Dye removal tests with the synthesized ZIF-8(C) were moved out as batch tests in 10 mL masks under magnetic stirring. For these experiments, 0.002-0.01 g of adsorbent were placed in 50 mL Erlenmeyer, including 10 mL of the dye solutions (10-400 mg/L), while agitating for an appropriate point of time (20-60 min) utilizing an acclimatized shaker at temperatures range of 25 to 65 K. The dye solutions had various *pHs* within 2 to 10. Finally, the adsorbent was separated from the aqueous solutions, by transferring the contents of Heerlen to centrifuging tubes for 30 min at 400 rpm. A UV-vis spectrophotometer (Cary 60, Agilent Technologies, and the USA) was utilized for analyzing the concentration of the reactive dye solution after adsorption. The solution *pH* was altered by appending a small quantity of NaOH or HCl. By ending the adsorption tests, by centrifugation, the adsorbent with adsorbed pigments was separated. After measurement, the concentration of dyes versus times the quantities of the

adsorbed dye at various times, (q_t, mg/g) and percent removal efficiency of reactive dye was obtained as:

(1) $\text{removal}\% = \frac{C_o - C_e}{C_o}$

(2) $q_t = \frac{(C_o - C_t) \times V}{m}$

Where C_0, C_e, and, C_t (mg/L) were the concentration of the reactive pigment, at initial, equilibrium, and at various times (t, min), respectively. V denotes the volume of the reactive dye solution, and m (g) represents the ZIF-8(C) mass. To estimate the adsorption capacity and assess kinetics features, the dosage attention of the adsorbent (0.002, 0.006, 0.008 and 0.01 g) and the initial dye solution's concentration (10, 20, 30, 50, 100,150, 200, 250, 300, 350 and 400 mg/L) were selected.

5. Result and discussion

5.1. Characterization of ZIF-8

Here we synthesized ZIF-8 by three methods and the material's textual features were determined by FT-IR, SEM, XRD, and nitrogen adsorption/desorption isotherm. To identify the phase structure of prepared ZIF-8(C), the X-ray diffraction pattern was illustrated in Fig. **2**. The diffraction signals at 2θ = 9.94° (011), 10.37° (002), 12.72° (112),14.73° (022),16.50° (013), 18.21° (022), 26.71° (134), 31.79° (235), and 36.27° (400) were observed and results displayed perfectly matched with the reported ZIF-8 XRD pattern [37].

The FT-IR spectra of synthesized ZIF-8(C) have been illustrated in Fig. **3** and confirmed the structure of synthesized ZIF-8(C). The peak of around 430 cm^{-1} corresponded to Zn–N coordination bonding [38].

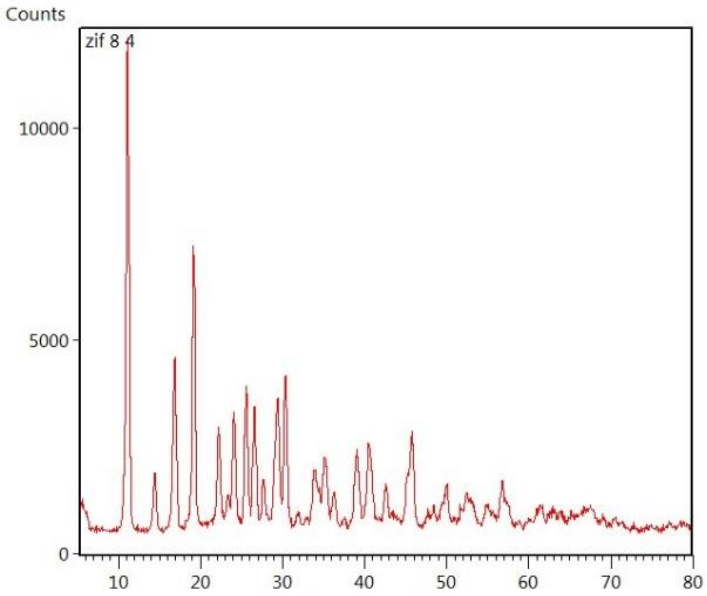

Fig. 2. XRD pattern of ZIF-8 (C)

The absorption band at 1585cm^{-1} was ascribed to the C=C chemical bond, and The asymmetric vibration band at 1146 cm^{-1} was attributed to the conjugated C–N vibrations. Absorption peaks at 3141cm^{-1} and 2929 cm^{-1} owing to the stretching vibrations of C–H bonds in the imidazole ring, and methyl group, respectively. The Fig. **4**, displays the N_2 adsorption-desorption analysis. The Langmuir isotherm showed that the adsorbed dye molecules were on the surface of ZIF-8(C) and had not entered into the holes of ZIF-8(C) (Fig. **5**). The obtained data of total pore volumes (V_{total} (Cm^3/g)) and BET specific surface area (S_{BET} (m^2/g)) were illustrated in Table **1**.

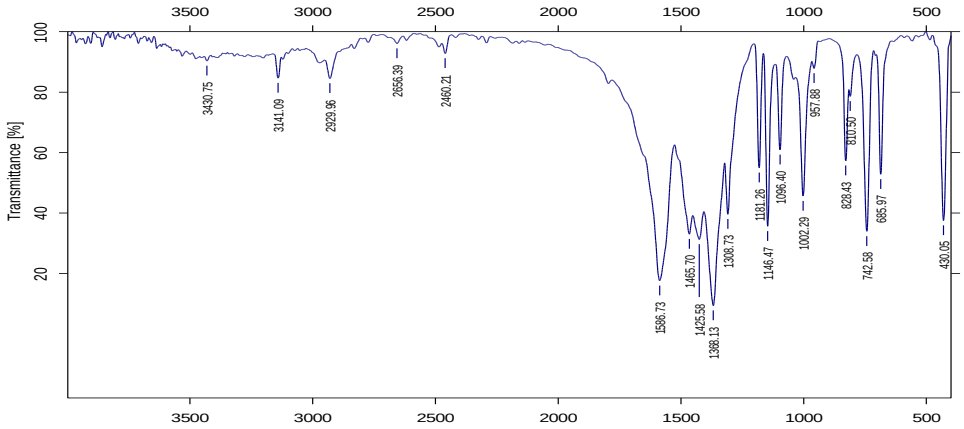

Fig. 3. FTIR spectra of ZIF-8(C)

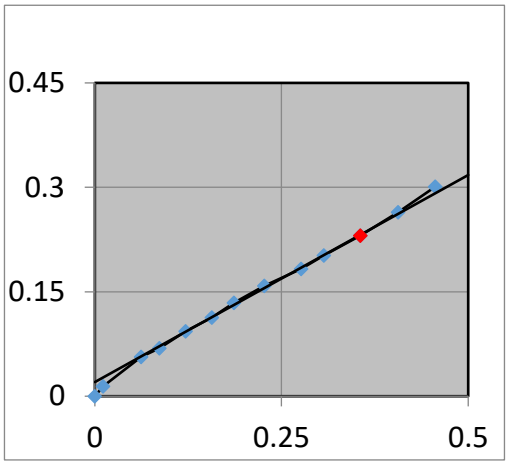

Fig. 5. Langmuir-plot of ZIF-8(C)

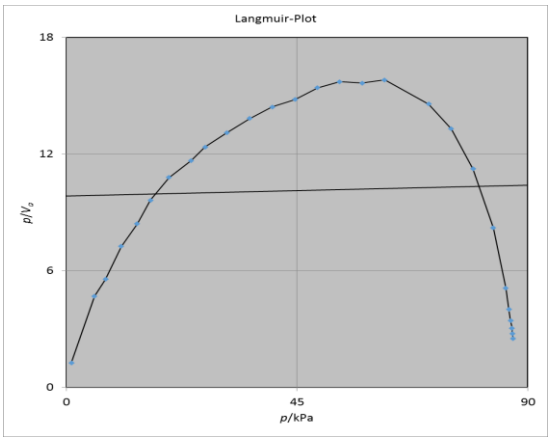

Fig. 4. BET plot of ZIF-8 (c)

Table 1. The results data of N_2 adsorption-desorption isotherms

Sample	S_{BET} (m^2/g)	V_{total} (Cm^3/g)
ZIF-8(C)	**701.39**	**161.15**

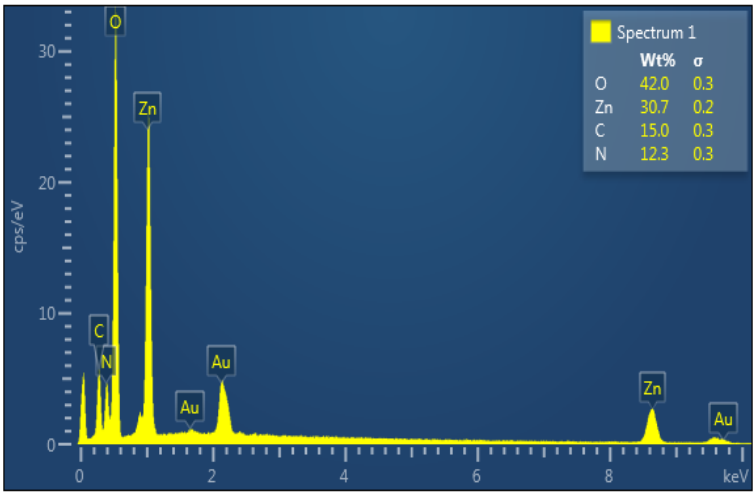

Fig. 6. EDX spectra of the ZIF-8 (C).

5.2. Adsorption of reactive dyes by ZIF-8(C)

5.2.1 Effects of solution pH

The investigation of the effect of pH on the adsorption procedure in the pH range of 2.0 to 10.0 was displayed in Fig. 8. At first, the studies of removing dyes using ZIF-8(C) were done with a dye concentration of 10 mg/L and the adsorbent dose of 0.01 g, at r.t. for 1 h. The data displayed that the maximum adsorption capacity of the ZIF-8(C) was achieved by decreasing the pH to 2, and it's due to an increase in the concentration of H^+ ions that enhanced electrostatic attraction between the dye molecule and the positively charged ZIF-8(C). Furthermore, at high *p*H conditions due to increasing the negatively charged ZIF-8(C), creating electrostatic repulsion between the active sites of the catalyst and OH^- of the dyes.

5.2.2 Effects of contact time

Another important parameter of the removal dye process is the examination of the contact time between the adsorbent and adsorbate. This study was at pH = 2 and 0.01 g adsorbent dosage for an initial dye concentration 10 mg/L, and 60 min was chosen because of the equilibrium time. As shown in Fig. **9**, Experiments exhibited that the amount of adsorbed dye increased

gradually with the rise of contact time. Frequently, the removal rate is initially fast, but it fades gradually with time until reaching equilibrium, and maybe it's due to increasing repulsive forces among the solute molecules on the bulk and solid phases over time (Fig. S2).

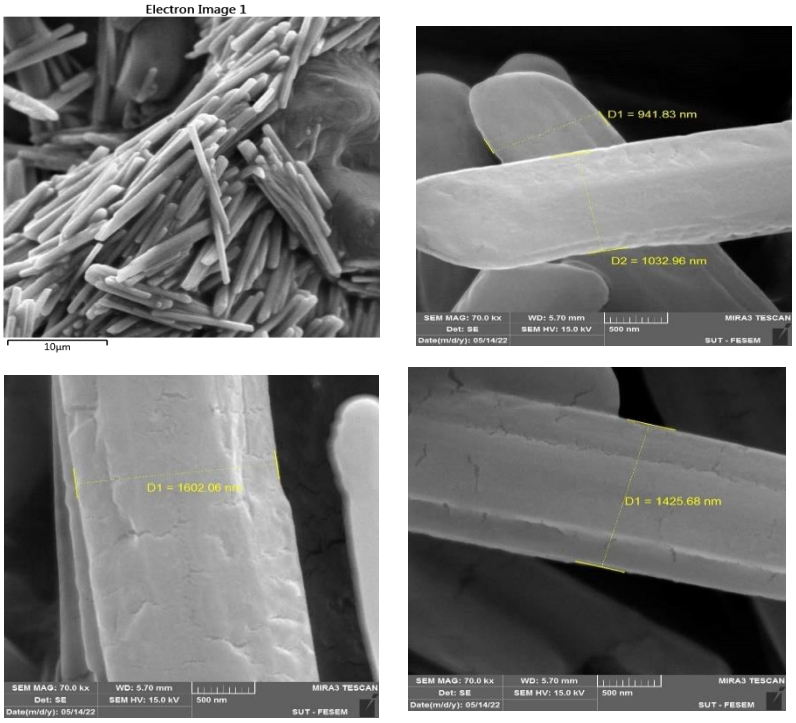

Fig. 7. SEM images of the ZIF-8 (C).

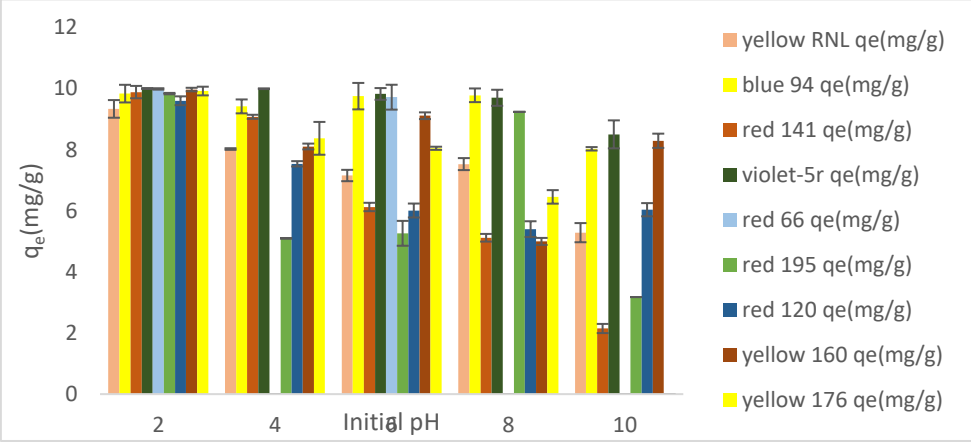

Fig. 8. Effect of pH of reactive dyes on adsorption

5.2.3 Effects of adsorbent dose on adsorption performance

The effect of the amount of ZIF-8(C) on the removal of dyes was examined. 0.002 g to 0.01g of adsorbent was utilized for adsorption tests at constant initial *p*H = 2, initial dye concentration 10 mg/L at room temperature for 60 min. The results indicated that the adsorption percentage incremented by raising the amount of ZIF-8(C), and when the amount exceeded 0.002 g, due to incremented surface area, and more adsorption sites available, the adsorption percentage reached 100 % (Fig. 10).

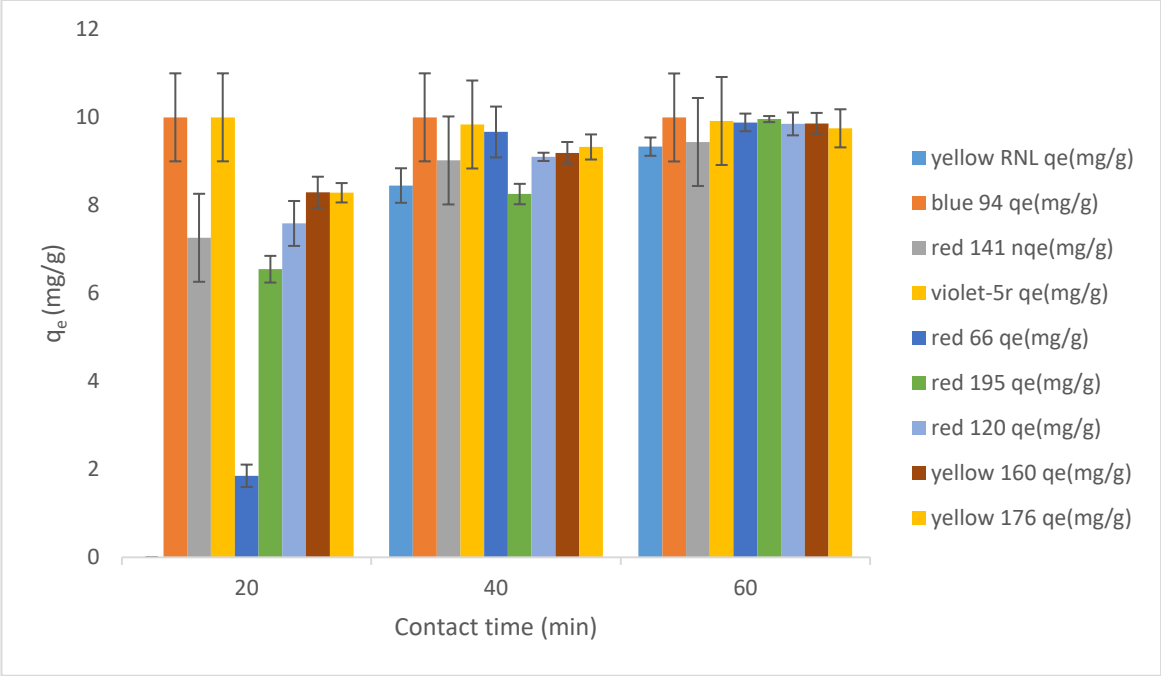

Fig. 9. Effect contact time of dyes on adsorption

5.2.4 Effect of temperature

The effects of temperature on the adsorption of dyes by ZIF-8(C) were assessed at direct pigment concentrations of 20 mg/L and *p*H = 2 with a stirring time of 60 min. The optimization of temperature for the adsorption procedure was at theش range of 25-65 °C (Fig. **11).** As data revealed, the maximum adsorption for three types of dyes (RD_2, RD_3, and RD_4) was at 65 °C, indicating the adsorption process's endothermic nature. On the other, increasing the temperature adversely affects removing other dyes (RD_1), (RD_5), (RD_6), (RD_7), (RD_8), and (RD_9) and maximum removal dye was achieved at 25 °C. Maybe for these six dyes with increasing the temperature, the adsorption capacity of ZIF-8(C) be reduced.

5.2.5 Effects of initial concentration of dyes

One of the most important parameters in the adsorption dye process is dye concentration. Hence, ZIF-8(C) was used to remove the different concentration ranges of the dyes. Studies were performed to assess the impacts of primary dye concentration on adsorption (25-65 °C) and 0.01g adsorbent concentration for 60 min. It was indicated that the adsorption of reactive dyes onto ZIF-8(C) is highly dependent on initial dye concentration, and when the initial reactive dyes concentration increments from 10 to 400 mg/L, the equilibrium sorption capacities of ZIF-8(C) were increased. Generally, the total number of possible adsorption sites is constant for a considered adsorbent dose, and the percent removal of reactive dyes diminishes by increasing the initial concentration. Hence, the larger ratio of the adsorbent's active adsorption sites is available at lower primary concentrations. Therefore, the dye's percentage removal is more prominent at lower initial concentrations; however, it is smaller at higher primary concentrations (Fig. S3).

5.3 Adsorption isotherm

The adsorption isotherm is the correlation function between the adsorbed pollutant amount and the equilibrium adsorbate concentration. Using equilibrium isotherms for the adsorption procedure, the relationship between the equilibrium concentration of the solution (C_e, mg/L) and the number of reactive dyes adsorbed on ZIF-8(C) material (q_e, mg/g) was determined. In this work for the analysis of equilibrium data, based on literature, the common adsorption isotherms mathematical models containing Langmuir (3-4) (Fig. S4), Freundlich (5-6) (Fig. S5), Tempkin (7) (Fig. S6), and Dubinin–Radushkevich (8-9) (Fig. S7) were studied [39].

$$\frac{1}{q_e} = \frac{1}{Q_{max}} + \frac{1}{bQ_{max}}\left(\frac{1}{C_e}\right) \quad (3)$$

$$R_L = 1/(1 + K_L C_0) \quad (4)$$

$$q_e = K_f C_e^{\frac{1}{n}} \quad (5)$$

$$\log q_e = \log K_f + \frac{1}{n}\log C_e \quad (6)$$

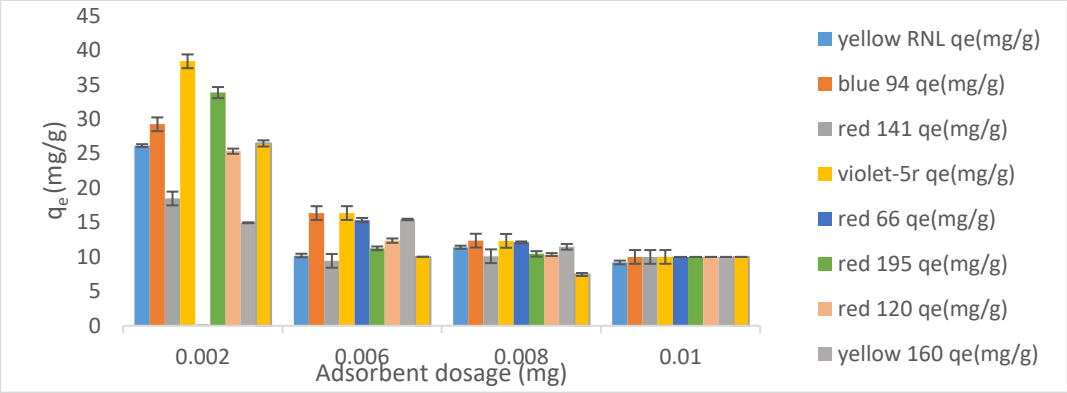

Fig. 10. Effect of adsorbent dose of reactive dyes on adsorption

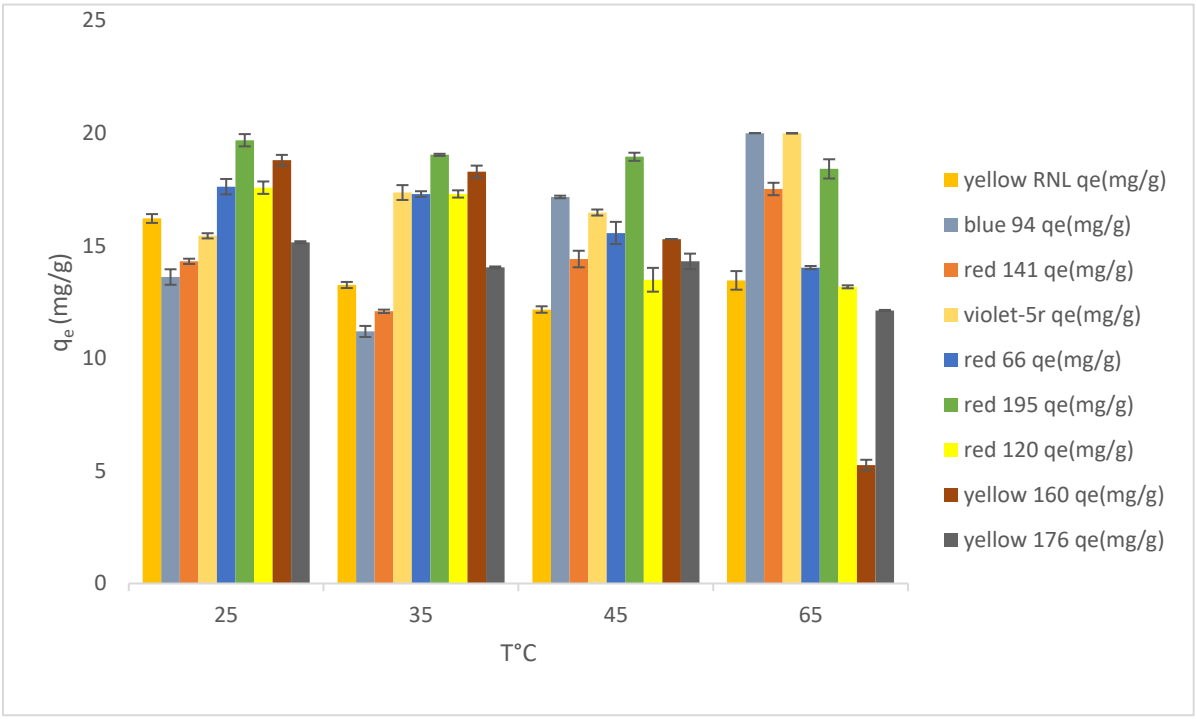

Fig. 11. Effect of temperature on adsorption

$$(7)\ q_e = \frac{RT}{b_T}\ln k_T + \frac{RT}{b_T}\ln C_e$$

$$(8)\ \ln q_e = \ln q_d - \beta\varepsilon^2$$

$$(9)\qquad \varepsilon = RT\ln\left(1+\frac{1}{C_e}\right)$$

The isotherm models were studied through four-parameter equations, and adsorption isotherm data (Table 2) showed the adsorption of the dye monolayer received by ZIF-8(C) which was consistent with the Langmuir isotherm model. Table **3** presents the comparison of our adsorbents' performance with the results of some recent reports on adsorbents regarding removing reactive dyes. The highest adsorption capacity of ZIF-8(C) for removal dyes were RD_1= 400, RD_2= 285.71, RD_3= 416.66, RD_4=416.66, RD_5= 303.03, RD_6= 270.27, RD_7= 666.66, RD_8= 200, RD_9= 101.01 mg/g. It can be concluded that the ZIF-8(C) possesses a relatively higher adsorption capacity revealing its applicability and feasibility as an effective, low-cost, and suitable adsorbent in the adsorption method for removing reactive dyes.

5.4 Adsorption kinetics study

Predicting the sorption rate is one of the most important factors in the batch adsorption process design, which is controlled by adsorption kinetics. Chemical kinetic models are based on the chemical and physical characteristics of the adsorbents. By investigating the kinetic uptake

Table 2. Linearized isotherm coefficients for dye adsorption at different adsorbents (0.01g) dosage and 50-400 mg/L dye concentrations (10 mL solution, pH=2, temperature =25-65°C, contact time time=60min).

Isoterm Models	Isoterm parameters	Remozal golden yellow RNL	Blue 94	Red 141	Violet-5r	Red 66	Red 195	Red120	Yellow 160	Yellow 176
Langmuir model	Q_m(mg/g) K_L (L/mg) R^2	400 0.0039 0.9974	285.71 0.0062 0.999	416.66 0.0042 0.9982	416.66 0.0039 0.9971	303.03 0.0065 0.9992	270.27 0.0051 0.9968	666.66 0.0022 0.9958	200 0.0081 0.986	101.01 0.0375 0.9817
Freundlich model	K_f (L/mg) n R^2	2.721 1.251 0.9921	4.056 1.422 0.9902	3.033 1.252 0.9941	3.142 1.283 0.9828	5.061 1.486 0.9757	3.649 1.459 0.9655	1.800 1.093 0.9942	3.618 1.467 0.9702	14.68 2.908 0.9794
Tempkin model	K_T(L/mg) b_T(J/mol) R^2 B_1	0.0620 36.76 0.9263 67.387	0.0755 48.75 0.9579 57.64	0.0667 39.65 0.9444 70.863	0.0680 41.86 0.963 67.126	0.0890 43.54 0.9879 56.894	0.0728 50.38 0.9638 49.177	0.0531 29.66 0.8877 83.527	0.0668 49.05 0.8276 50.505	0.3449 115.52 0.9678 21.447
Dubinin-Radushkevich model	Q_d(mg/ g) β(mol^2/J^2) E (kJ/ mol) R^2	140.62 0.00009 0.074 0.8446	134.41 0.0001 0.070 0.874	148.81 0.0001 0.070 0.8488	146.46 0.0001 0.070 0.8626	140.59 0.00007 0.0845 0.8973	119.74 0.0001 0.070 0.9027	153.57 0.0001 0.070 0.8086	114.52 0.0001 0.070 0.7921	87.49 0.0000 3 0.129 0.8802
Separation factor (R_L)	C_0 (mg/L) 50 400	0.836 0.390	0.763 0.287	0.826 0.373	0.836 0.390	0.754 0.277	0.796 0.328	0.900 0.531	0.711 0.235	0.347 0.0625

Table 3. Comparison of the adsorption capacity of reactive dyes by various adsorbents.

Adsorbents samples	q_{max} (mg/g)	Ref
Remazol golden yellow RNL		
RYG lop	5.63 ± 0.09	[40]
New ZIF-8(C)	400	This study
Red 141		
Pyrrhotite Ash	5.07	[41]
Nickel oxide doped	38.91	[41]
Comcob activated carbon	2.86	[42]
New ZIF-8(C)	416.66	This study
Violet_5r		
Activated coal obtains from orange peel	185.1	[43]
Bent-NH_2/TOL	30.9	[44]
Bent-NH_2/HEX	60.9	[44]
New ZIF-8(C)	416.66	This study
Yellow 176		
HDTMA-zeolite	13.148	[45]
CTAB-zeolite	5.539	[45]
Biomass fly ash	3.65	[46]

New ZIF-8(C)	101.01	This study
Red 120		
Jatropha curcas shell treated by non-thermal plasma	85.3	[47]
Functionalized sludge	46.8	[48]
New ZIF-8(C)	666.66	This study
Red 195		
NaOH treated jute fibre	270.27	[49]
Chisotan/polyanilline-chitosan	37.87/106.383	[50]
BV_{16}	7.3	[51]
New ZIF-8(C)	250	This study
Yellow 160		
Industrial Wastewater onto Modified Sand Aqueous	50	[52]
CAPB-NC	54.61±7.16	[53]
New ZIF-8(C)	200	This study

capacity against contact time, adsorption mechanisms and rates can be defined. In the present work, experimental conditions were optimized as initial concentrations of 10 and 400 mg/L, solution *pH* =2, and a dose of 1 g/L for reactive dyes. The adsorption capacities first incremented and then remained constant, with equilibrium times of 60 min for 10-400 solutions. The equilibrium adsorption capacity increased from 10 mg/g with the increasing dye concentrations, for example; RD_1=190, RD_2=180, RD_3=200, RD_4=183.46, RD_5=175, RD_6 =156.23, RD_7=220.3, RD_8 =172.22, RD_9 =100 mg/g this indicated that high dyes removal concentrations could lead to auspicious adsorption. In this work for a better estimate of dye adsorption kinetics over the treated adsorbents, the dye adsorption kinetics were studied via the first- order reaction model was used in terms of the solution concentration (10) (Fig. S8), pseudo-first-order equation of Lagergren et al. in terms of the solid capacity (11) (Fig. S9), pseudo-second-order oriented by the solid phase sorption (12), second-order reaction model, based on the solution concentration (13) (Fig. S10), intra-particle diffusion (14) (Fig. S11), and Elovich models (15) (Fig. S12) [54].

$$\ln C_t = \ln C_0 - k_1 t \quad (10)$$

$$\ln(q_e - q_t) = \ln q_e - k s_1 t \quad (11)$$

$$\frac{t}{q_t} = \frac{1}{h} + \frac{1}{q_e} t \quad (12)$$

$$\frac{1}{C_t} - \frac{1}{C_0} = k_2 t \quad (13)$$

$$q_t = k_p t^{1/2} + I \quad (14)$$

$$q_t = \frac{1}{\beta} \ln(\alpha\beta) + \ln(t) \quad (15)$$

The linear plot of t/q_t against time (t) for the adsorption of dyes by ZIF-8(C) based on pseudo-second-order kinetic was indicated in The summary of obtained data of these studies was illustrated in Table **4**.

The results show that the R^2 amounts of the pseudo-second-order model (R^2 value: RD_1=0.9872, RD_2=0.9812, RD_3=0.9978, RD_4=0.9986, RD_5=0.994, RD_6=0.9962, RD_7=0.9713, RD_8=0.9828, RD_9=0.9752) has higher correlation coefficient than the other models.

5.5 Thermodynamic study

The value of the thermodynamic study is in the discovery of the different parameters such as the standard enthalpy ΔH° (kJ/mole), formal free energy ΔG° (kJ/mole), and standard entropy ΔS°(J/mole .K), presenting a precise explanation of the adsorption procedure through the practical application. The thermodynamic parameters are determined through equations [55]:

(16) $$\mathrm{Ln}K_d = \Delta S^\circ/R - \Delta H^\circ/RT$$

(17) $$K_d = (C_o - C_a) * V/(C_o * m)$$

(18) $$\Delta G^0 = -RT\mathrm{Ln}K_d$$

The advantages of ΔS° and ΔH° were arranged from the intercept and slope of the van Hof plot of ln k_d against 1/T (**Fig. S14**). Table **5** shows the values of the various thermodynamic parameters for dye. Positive ΔG° values obtained at temperature for (RD_8) indicated the feasibility and the nonspontaneous nature of dye removal adsorption ZIF-8(C). Negative ΔG° values obtained at all temperatures RD_1, RD_2, RD_3, RD_4, RD_5, RD_6, RD_7, and RD_9 (Table 4) revealed the feasibility and the spontaneous nature of dye removal adsorption by ZIF-8(C). For RD_2, RD_3, and RD_4 that are all negative. It was indicated that the adsorption of reactive dyes to ZIF-8(C) could spontaneously occur at these examined temperatures.

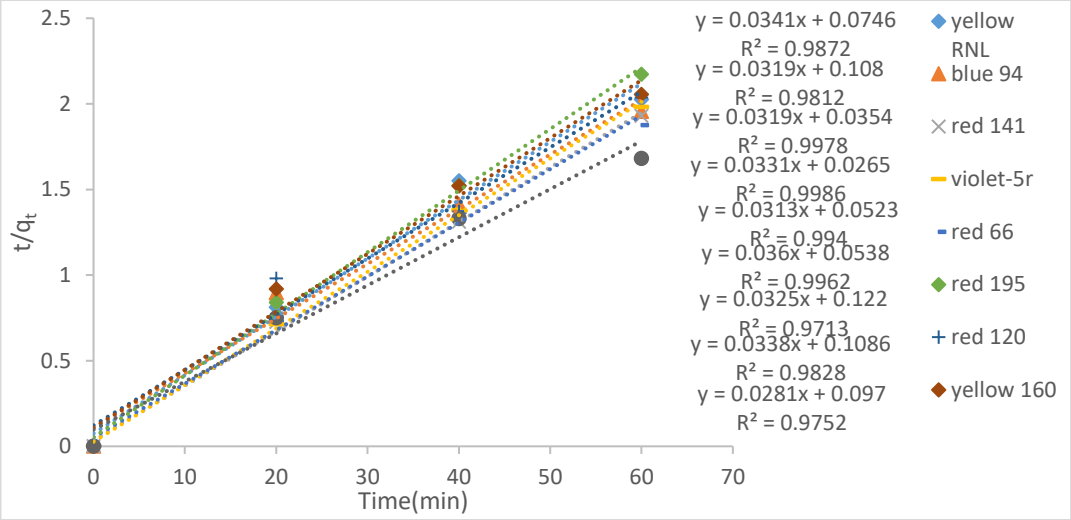

Fig. 12. Kinetics plot for the adsorption of reactive dyes bye ZIF-8(C)

Table 4. Kinetics constants for the adsorption of reactive dyes by ZIF-8(C) (contact time=20-60 min, temperature=25-65°C, stirring=400 rpm and pH=2) (Fig. S13).

		Remazol golden yellow RNL	Blue 94	Red 141	Violet-5r	Red 66	Red 195	Red 120	Yellow 160	Yellow 176
Pseudo – first – order model	**$q_{e,exp}$(mg/g)**	29.62	30.67	31	30.27	31.99	27.62	29.48	29.19	35.63
	$q_{e,cal}$(mg/g)	22.90	28.78	22.47	21.15	25.10	23.63	41.51	27.02	30.82
	K_1(min^{-1})	0.0506	0.0557	0.0614	0.0783	0.0617	0.0754	0.1101	0.0575	0.0463
	R^2	0.8382	0.9905	0.8302	0.8645	0.8963	0.9723	0.9321	0.9879	0.9343
first – order model	**C_0**	42.36	43.84	40.46	39.64	42.84	42.13	44.37	44.05	43.29
	K_1	0.0136	0.0152	0.0147	0.0141	0.0163	0.0126	0.0151	0.0141	0.0196
	R^2	0.8015	0.892	0.7446	0.6933	0.8725	0.7635	0.8758	0.8811	0.9149
Pseudo – second – order model	**$q_{e,cal}$(mg/g)**	29.32	31.34	31.34	30.21	31.94	27.77	30.76	29.58	35.58
	K_2(g/min.mg)	0.0155	0.009	0.0287	0.0413	0.0187	0.0241	0.0086	0.0105	0.0081
	R^2	0.9872	0.9812	0.9978	0.9986	0.994	0.9962	0.9713	0.9828	0.9752
second – order model	**C_0**	41.66	44.44	38.75	37.17	42.73	40.81	44.44	43.85	45.45
	K_2	0.0004	0.0005	0.0005	0.0005	0.0006	0.0004	0.0005	0.0005	0.0008
	R^2	0.8682	0.9617	0.7882	0.7371	0.9447	0.8181	0.9078	0.9418	0.9729
Intra-particle diffusion model	**K_p(g/min.mg)**	1.4764	2.5559	1.0304	0.6567	1.356	1.2021	2.904	2.2798	2.7921
	C(mg/g)	17.538	11.007	22.592	25.047	21.211	18.448	8.3629	11.652	13.418
	R^2	0.8527	0.9981	0.8663	0.9617	0.9631	0.9894	0.8388	0.9981	0.9609
Elovich constants	**R^2**	0.7997	0.9993	0.8151	0.9303	0.9322	0.9989	0.8869	0.9993	0.9293
	α (Mg/g.min)	64.97	7.31	1505.80	227595.47	200.85	140.98	4.85	8.56	9.92
	ß (g/mg)	0.237	0.132	0.339	0.524	0.254	0.280	0.113	0.148	0.123

The ΔG°, the temperature rose become even more negative, indicating that the higher temperature was more satisfactory for the RD_2, RD_3, and RD_4 adsorptions. ΔS° and ΔH° were found to be 104.25, 36.24, 90.78 j/mol. K and 34.33, 9.31, 30.69 kJ/ mol, respectively for the RD_2, RD_3, and RD_4. Since ΔH° was positive, the validation of adsorption of RD_2, RD_3, and RD_4 to ZIF-8(C) was considered as an endothermic reaction. The positive ΔS° value, desorption of various pre-adsorbed water molecules is also suggested over the adsorption of RD_2, RD_3, and RD_4 molecules to ZIF-8(C). Such analyses are consistent with the findings of the adsorption isotherm and kinetics. The endothermic adsorption to ZIF-8(C) was strongly related to the chemical interaction. Mainly, the adsorption phenomenon is physical owing to the lower adsorption activation enthalpy for reactive dyes RD_1, RD_5, RD_6, RD_7, RD_8, and RD_9. For reactive dyes (RD_1, RD_5, RD_6, RD_7, RD_8, RD_9), the enthalpy (−ΔH°) was attained, and the negative value suggested that the adsorption was an exothermic procedure. The negative value of ΔS° also suggests that it reduces irregularities. ΔH° and ΔS° = (RD_1: -9.07/-17.53, RD_5: -12.93/-32.34, RD_6: -17.03/-44.07, RD_7: -12.15/-34.78, RD_8: -45.60/-146.00, RD_9:-9.17/-24.52) (**Table 5**).

Table 5. Thermodynamic parameters for the adsorption of reactive dyes on ZIF-8(C)

ΔS° (J/mol.K)	**ΔH°(Kj/mol)**	**ΔG°(Kj/mol)**	**(k)**	**(RNL) (PPM)**
-17.53	-9.07	-3.65	298	30mg/L
		-3.45	318	
		-2.91	338	
ΔS° (J/mol.K)	ΔH°(Kj/mol)	ΔG°(Kj/mol)	(k)	(Blue 94) (PPM)
104.25	34.33	2.40	298	30 mg/L
		1.27	318	
		-1.91	338	
ΔS°/(J/mol.K)	ΔH°(Kj/mol)	ΔG°(Kj/mol)	(k)	(Red141) (PPM)
36.24	9.31	-0.99	298	30 mg/L
		-1.16	318	
		-2.49	338	
ΔS°(J/mol.K)	ΔH°(Kj/mol)	ΔG°(Kj/mol)	)k(	(Violet-5r) (PPM)
90.78	30.69	2.65	298	30 mg/L
		2.38	318	
		-1.13	338	
ΔS°(J/mol.K)	ΔH°(Kj/mol)	ΔG°(Kj/mol)	(k)	(Red 66) (PPM)
-32.34	-12.93	-3.18	298	30 mg/L
		-2.47	318	
		-1.85	338	
ΔS°(J/mol.K)	ΔH°(Kj/mol)	ΔG°(Kj/mol)	(k)	(Red195) (PPM)
-44.07	-17.03	-3.63	298	30 mg/L
		-2. 72	318	
		-1.82	338	
ΔS°(J/mol.K)	ΔH°(Kj/mol)	ΔG°(Kj/mol)	(k)	(Red 120) (PPM)
-34.78	-12.15	-1.80	298	30 mg/L
		-0.45	318	
		-0.40	338	
ΔS°(J/mol.K)	ΔH°(Kj/mol)	ΔG°(Kj/mol)	(k)	(Yellow 160) (PPM)
-146.00	-45.60	-1.00	298	30
		0.23	318	
		4.12	338	
ΔS°(J/mol.K)	ΔH°(Kj/mol)	ΔG°(Kj/mol)	)k(	(Yellow 176) (PPM)
-24.52	-9.17	-1.66	298	30
		-1.27	318	
		-0.65	338	

Table 6: Removal of Red 120 dye from textile wastewater sample.

dye	Initial concentration (mg/L)	Final concentration (mg/L)	% Removal
Red 120	50	5	90

5.6 Adsorption mechanism

The ZIF-8 surface was reported as positively charged [56]. The negatively charged sulfonic acid groups in the received dye molecule were adsorbed readily over the ZIF-8(C) with a positive charge (Fig. S15). For reactive dyes, these superior adsorption features of ZIF-8(C) were dependent highly on their exclusive structures and the interaction between active functional groups like π-π conjugation, electrostatic interaction, and metal coordination (all dyes) effect (Fig. S16).

5.7 Remove dyes from real samples

The ability and potential of synthesized catalyst can be shown better by examination of the removal of dyes from real wastewater. In this work, wastewater samples were filtered with a 0.45-mm pore-size membrane filter to remove suspended particulate matter, and the process was according to our previous reports [57]. As shown in Table **6**, the proposed method could be applied successfully for the removal of Red 120 in textile wastewater sample with acceptable efficiency.

5.8 The BOD and COD analysis

The COD and BOD analysis of wastewater were measured by Arman mohit pak Iranian company. The initial levels of COD and BOD were 1910 and 810 mg/L, respectively. After treatment, the amounts of COD and BOD were decreased to 61 and 33 mg/L. The data indicates the efficient performance of ZIF-8(C).

5.9 Recycle and regeneration of ZIF-8(C) nanocomposites

The recovery and reusability are among the most important properties of catalysts. After decolorization of the wastewater samples, ZIF-8(C) was separated by centrifugation and washed with 0.1 mol/L NaOH in 50% aqueous ethanol solution, dried in a vacuum oven, and then reused directly for the next adsorption. Although the adsorption of dye, was gradually reduced by improving in desorption cycles, the recreated adsorbents still revealed good performance for their adsorption after first-cycle regeneration. In Fig. **13**, there usability of ZIF-8(C) after the four runs is still outstanding, representing the original capacity of 95, 85, and 75% (RD_2, RD_6, and RD_7), revealing the cost-effective prepared adsorbent.

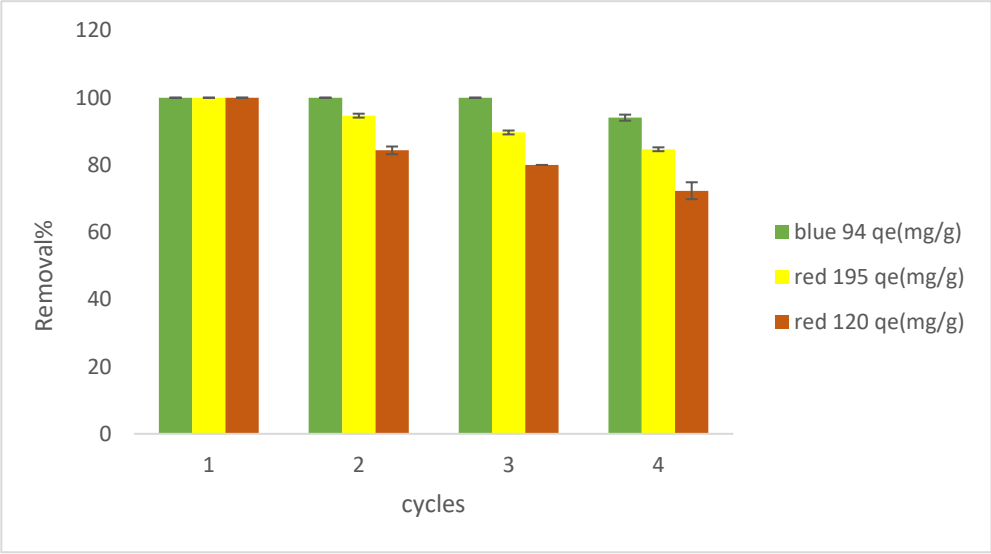

Fig. 13. Recycled adsorption of RD_2, RD_6 and RD_7 (20 mg/L,by ZIF-8(C) 0.01 g).

XRD patterns of ZIF-8(C) composites before and after adsorption showed that the peaks shape of ZIF-8(C) after the adsorption of dyes was according to ZIF-8(C) before adsorption, revealing that adsorption failed to alter the crystalline form of ZIF-8(C) (Fig. S17).

6. Conclusions

In this summary, the zeolitic-imidazolate framework, ZIF-8(C), has been prepared with three different methods containing the conventional solvothermal, ultrasonic assisted solvothermal, and mechanochemical method, and results showed that the best yield was obtained by the mechanochemical method. The optimum conditions were indicated by the response surface methodology-based optimization results to remove the chosen reactive dyes: (RD_1), (RD_2), (RD_3), (RD_4), (RD_5), (RD_6), (RD_7), (RD_8) and, (RD_9) (C_0 =10 mg/L, dose = 1g/L, contact time = 60 min). ZIF-8(C) could also be recovered through the straightforward, simple washing procedure, and the catalyst could be reused for at least four cycles under optimized conditions without significant loss of its catalytic activity. Factors affecting the adsorption capacity including mixing time, temperature, adsorbent dose, initial concentration, and pH were investigated. Various isotherm data were analyzed and the Langmuir model was found as the most appropriate model. The adsorption kinetics models were investigated and the adsorption kinetics followed the pseudo-second-order for all dyes. After determining the optimal conditions, the effectiveness of ZIF-8(C) in decolorizing real textile wastewater samples was evaluated, demonstrating exceptional performance. The levels of BOD and COD in the real textile wastewater were significantly reduced after using ZIF-8(C).

7. Acknowledgements

The author would like to thank Islamic Azad University of Yadegar-e-Imam Khomeini (RAH) Shahre-rey branch for giving grant to carry out the above-mentioned project.

8. Supplemental information

Supplemental information can be found online

Reference

[1] D. Sun, X. Zhang, Y. Wu, X. Liu, Adsorption of anionic dyes from aqueous solution on fly ash. *J. Hazard. Mater. 181* (2010), 335–342. https://doi.org/10.1016/j.jhazmat.2010.05.015

[2] A. Sharma, Z. Syed, U. Brighu, A.B. Gupta, C. Ram, Adsorption of textile wastewater on alkali-activated sand. *J. Clean. Prod. 220* (2019), 23–32. https://doi.org/10.1016/j.jclepro.2019.01.236

[3] M. Rohani Moghadam, S. Pirozi, F. Beigmoradi, A. Bazmandegan-Shamili, H. Masoodi, Application of response surface methodology for modeling and optimization of Basic Yellow 28 decolorization using sonoelectrochemistry. *Chem. Rev. Lett., 6* (2022),15-23. https://doi.org/10.22034/CRL. 2023.381956.1197.

[4] P. Karacakaya, N.K. Kılıç, E. Duygu, G. Dönmez, Stimulation of reactive dye removal by cyanobacteria in media containing triacontanol hormone. *J. Hazard. Mater. 172* (2009)., 1635–1639. https://doi.org/10.1016/j.jhazmat.2009.08.037

[5] J. Paul, K.P. Rawat, K.S.S. Sarma, S. Sabharwal, Decoloration and degradation of Reactive Red-120 dye by electron beam irradiation in aqueous solution. *Appl. Radiat. Isot. 69* (2011), 982–987. https://doi.org/10.1016/j.apradiso.2011.03.009

[6] S. Khammarnia, J. Saffari, M.S. Ekrami-Kakhki, Synthesis of $La_2MnFe_2O_7$ and $La_2CuFe_2O_7$ Magnetic Nanocomposites (Nano Mixed Metal Oxides) as Efficient Photocatalyst for Organic Dye Removal. *Chem. Rev. Lett., 7* (2024), 123-133. https://doi.org/10.22034/crl.2024.434922.1277

[7] S. Arabi, Adsorption of Orange 3R by chitosan modified montmorillonite nanocomposite. *Chem. Rev. Lett., 6* (2022), 55-65. https://doi.org/10.22034/crl.2023.387842.1208

[8] R. Mohammadi, Highly Efficient catalyst of TiO_2/chitosan for Photodegradation and Sonodegradation of Organic Pollutants. *Chem. Rev. Lett., 5* (2022), 133-140.https://doi.org/10.22034/crl.2022.320844.1143

[9] M. Kalhor, Z. Orouji, M. Khalaj, 4-Methylpyridinium chloride ionic liquid grafted on Mn@zeolite-Y: Design, fabrication and performance as a novel multi-functional nanocatalyst in the four-component synthesis of pyrazolophthalazine-diones. Micropor. *Mesopor. Mater. 329* (2022), 111498. https://doi.org/ 10.1016/j.micromeso.2021.111498.

[10] M. Khalaj, M. Zarandi, A Cu (II) complex supported on Fe_3O_4@SiO_2 as a magnetic heterogeneous catalyst for the reduction of environmental pollutants. RSC Adv. 12 (2022), 26527.https://doi.org/ 10.1039/d2ra04787j.

[11] M. Khalaj, Preparation of benzo[4,5]thiazolo[3,2-a]chromeno[4,3-d] pyrimidin-6-one derivatives using MgO-$MgAl_2O_4$ composite nano-powder. *Arab. J. Chem. 13* (2020), 6403-6411. https://doi.org/10.1016/j.arabjc.2020.05.041.

[12] A. Mathew, S. Parambadath, M.J. Barnabas, H.J. Song, J.S. Kim, S.S. Park, C.S. Ha, Rhodamine 6G assisted adsorption of metanil yellow over succinamic acid functionalized MCM-41. *Dyes Pigm. 131* (2016), 177–185. https://doi.org/10.1016/j.dyepig.2016.04.007.

[13] L. Hajiaghababaei, A. Sharafi, S. Suzangarzadeh, F. Faridbod, Mercury recognition: A potentiometric membrane sensor based on 4-(benzylidene amino)-3, 4-dihydro-6-methyl-3-thioxo-1, 2, 4-triazin-5 (2H) one. Anal. Bioanal. Electrochem 5 (2013), 481-493.https://www.magiran.com/volume/93177

[14] L. Hajiaghababaei, A. Badiei, M. Shojaan, M.R. Ganjali, G. M. Ziarani, P. Zarabadi-Poor, A novel method for the simple and simultaneous preconcentration of Pb 2+ , Cu 2+ and Zn 2+ ions with aid of diethylenetriamine functionalized SBA-15 nanoporous silica compound. *J. Environ. Anal. Chem. 92* (2012), 1352–1364. https://doi.org/10.1080/03067319.2011.585715

[15] L. Hajiaghababaei, A.S. Shahvelayati, S.A. Aghili, Rapid determination of cadmium: a potentiometric membrane sensor based on ninhydrin-pyrogallol monoadduct as a new ionophore. Anal. Bioanal. Electrochem 7 (2015), 91-104. http://abechem.ir/No.%201-2015/2015,%207(1),%2091-104.pdf

[16] S. Hadadian, L. Dolatyari, B. Farajmand, M.R. Yaftian, Methylene blue elimination from contaminated water solutions using a polyvinyl chloride based polymer inclusion membrane containing bis (2-ethylhexyl) phosphoric Acid. *Chem. Rev. Lett., 7* (2024), 311-324. https://doi.org/10.22034/crl.2024.437064.1287.

[17] K. Silas, Y.P. Musa, M.D. Habiba, Effective application of Jatropha curcas husk activated $ZnCl_2$ for adsorption of methylene blue: isotherm, kinetics and development of empirical model. *Chem. Rev. Lett., 5* (2022), 153-160. https://doi.org/10.22034/CRL.2022.319848.1140.

[18] F.Z. Benhachem, T. Attar, F. Bouabdallah, Kinetic study of adsorption methylene blue dye from aqueous solutions using activated carbon. *Chem. Rev. Lett., 2* (2019), 33-39. https://doi.org/10.22034/crl.2019.87964.

[19] C. Janiak, J.K. Vieth, MOFs, MILs and more: concepts, properties and applications for porous coordination networks (PCNs). *New J. Chem. 34* (2010), 2366. https://doi.org/10.1039/c0nj00275e

[20] S. Zheng, X. Li, B. Yan, Q. Hu, Y. Xu, X. Xiao, H. Pang, Transition-Metal (Fe, Co, Ni) Based Metal-Organic Frameworks for Electrochemical Energy Storage. *Adv. Energy Mater. 7* (2017), 2366. https://doi.org/10.1002/aenm.201602733

[21] L. Li, S. Tang, C. Wang, X. Lv, M. Jiang, H. Wu, X. Zhao, High gas storage capacities and stepwise adsorption in a UiO type metal–organic framework incorporating Lewis basic bipyridyl sites. *Chem. Comm. 50* (2014), 2304. https://doi.org/10.1039/c3cc48275h.

[22] C.-Y. Gao, H.-R. Tian, J. Ai, L.-J Li, S. Dang, Y.-Q Lan, Z.-M. Sun, A microporous Cu-MOF with optimized open metal sites and pore spaces for high gas storage and active chemical fixation of CO_2. *Chem. Comm. 52* (2016), 11147–11150. https://doi.org/10.1039/C6CC05845K.

[23] J. Duan, M. Higuchi, J. Zheng, S. Noro, I.-Y Chang, K. Hyeon-Deuk, S. Kitagawa, Density Gradation of Open Metal Sites in the Mesospace of Porous Coordination Polymers. *J. Am. Chem. Soc. 139* (2017), 11576–11583. https://doi.org/10.1021/jacs.7b05702.

[24] D. Chen, S. Chen, Y. Jiang, S. Xie, H. Quan, L. Hua, L. Guo, Heterogeneous Fenton-like catalysis of Fe-MOF derived magnetic carbon nanocomposites for degradation of 4-nitrophenol. *RSC Adv. 7* (2017), 49024–49030. https://doi.org/10.1039/C7RA09234B.

[25] Z. Hasan, J.W. Jun, S.H. Jhung, Sulfonic acid-functionalized MIL-101(Cr): An efficient catalyst for esterification of oleic acid and vapor-phase dehydration of butanol. *J. Chem. Eng. 278* (2015), 265–271. https://doi.org/10.1016/j.cej.2014.09.025.

[26] C. Zhang, K. Huang, MOF-derived iron as an active energy storage material for intermediate-temperature solid oxide iron–air redox batteries. *Chem. Comm. 53* (2017), 10564–10567. https://doi.org/10.1039/C7CC06131E.

[27] J. Linnemann, L.Taudien, M. Klose, L. Giebeler, Electrodeposited films to MOF-derived electrochemical energy storage electrodes: a concept of simplified additive-free electrode processing for self-standing, ready-to-use materials. *J. Mater. Chem. 5* (2017). 18420–18428. https://doi.org/10.1039/C7TA01874F.

[28] E. Shearier, P. Cheng, Z. Zhu, J. Bao, Y.H. Hu, F. Zhao, Surface defection reduces cytotoxicity of Zn (2-methylimidazole)$_2$ (ZIF-8) without compromising its drug delivery capacity. *RSC Adv. 6* (2016), 4128–4135. https://doi.org/10.1039/C5RA24336J.

[29] S. Wuttke, A. Zimpel, T. Bein, S. Braig, K. Stoiber, A. Vollmar, S. Meiners, Validating Metal-Organic Framework Nanoparticles for Their Nanosafety in Diverse Biomedical Applications. *Adv. Healthc. Mater. 6* (2017), 4128–4135. https://doi.org/10.1002/adhm.201600818

[30] A.a. Mohammadi, A. Alinejad, B. Kamarehie, S. Javan, A. Ghaderpoury, M. Ahmadpour, M. Ghaderpoori, Metal-organic framework Uio-66 for adsorption of methylene blue dye from aqueous solutions. *Int. J. Environ. Sci. Technol. 14* (2017), 1959–1968. https://doi.org/10.1007/s13762-017-1289-z

[31] K. Wang, C. Li, Y. Liang, T. Han, H. Huang, Q. Yang, C. Zhong, Rational construction of defects in a metal–organic framework for highly efficient adsorption and separation of dyes. *J. Chem. Eng. 289* (2016), 486–493. https://doi.org/10.1016/j.cej.2016.01.019

[32] R. Rajak, M. Saraf, A. Mohammad, S.M. Mobin, Design and construction of a ferrocene based inclined polycatenated Co-MOF for supercapacitor and dye adsorption applications. *J. Mater. Chem. 5* (2017). 17998–18011. https://doi.org/10.1039/C7TA03773B

[33] J. Cravillon, S. Münzer, S.-J. Lohmeier, A. Feldhoff, K. Huber, M. Wiebcke, Rapid Room-Temperature Synthesis and Characterization of Nanocrystals of a Prototypical Zeolitic Imidazolate Framework. *Chem. Mat. 21* (2009), 1410–1412. https://doi.org/10.1021/cm900166h

[34] F. Tian, A.M. Cerro, A.M. Mosier, H.K. Wayment-Steele, R.S. Shine, A. Park, L. Benz, Surface and Stability Characterization of a Nanoporous ZIF-8 Thin Film. *J. Phys. Chem. 118* (2014), 14449–14456. https://doi.org/10.1021/jp5041053

[35] J. Cravillon, C.A. Schröder, H. Bux, A. Rothkirch, J. Caro, M. Wiebcke, Formate modulated solvothermal synthesis of ZIF-8 investigated using time-resolved in situ X-ray diffraction and scanning electron microscopy. *Cryst. Eng. Comm. 14* (2012), 492–498. https://doi.org/10.1039/C1CE06002C

[36] K. S. Park, Z. Ni, A.P. Côté, J.Y. Choi, R. Huang, F.J. Uribe-Romo, O.M. Yaghi, Exceptional chemical and thermal stability of zeolitic imidazolate frameworks. *Proc. Natl. Acad. Sci. 103* (2006), 10186–10191. https://doi.org/10.1073/pnas.0602439103

[37] M.R. Kim, T. Kim, H.S. Rye, W. Lee, H.-G Kim, M.I. Kim, C.-S. Lim, Zeolitic imidazolate framework promoters in one-pot epoxy–amine reaction. *J. Mater. Sci. 55* (2020), 2068–2076. https://doi.org/10.1007/s10853-019-04111-5

[38] M. Adnan, K. Li, L. Xu, Y. Yan, X-Shaped ZIF-8 for Immobilization Rhizomucor miehei Lipase via Encapsulation and Its Application toward Biodiesel Production. *Catalysts 8* (2018), 96. https://doi.org/10.3390/catal8030096

[39] I. Langmuir, The Adsorption of Gases on Plane Surface of Glass, Mica and Olatinum. J. Am. Chem. Soc. 40 (1918), 1361-1403. http://dx.doi.org/10.1021/ja02242a004

[40] G.E.D Nascimento, M.M.M.B. Duarte, N.F. Campos, O.R.S.D Rocha, V.L.D Silva, Adsorption of azo dyes using peanut hull and orange peel: a comparative study. *Environ. Technol. 35* (2014), 1436–1453. https://doi.org/10.1080/09593330.2013.870234

[41] J. Mouldar, B. Hatimi, H. Hafdi, M. Joudi, M.E.A. Belghiti, H. Nasrellah, M. Bakasse, Pyrrhotite Ash Waste for Capacitive Adsorption and Fixed-Bed Column Studies: Application for Reactive Red 141 Dye. *Water Air Soil. Pollut. 231*(2020), 205. https://doi.org/10.1007/s11270-020-04578-y

[42] T.H. Nazifa, N. Habba, A. Salmiati, T. Hadibarata, Adsorption of Procion Red MX-5B and Crystal Violet Dyes from Aqueous Solution onto Corncob Activated Carbon. *J. Chin. Chem. Soc. 65* (2018), 259–270. https://doi.org/10.1002/jccs.201700242

[43] R. Foroutan, M. Ahmadlouydarab, B. Ramavandi, R. Mohammadi, Studying the physicochemical characteristics and metals adsorptive behavior of CMC-g-HAp/Fe3O4 nanobiocomposite. *J. Environ. Chem. Eng. 6* (2018), 6049–6058. https://doi.org/10.1016/j.jece.2018.09.030

[44] L.N.F. Queiroga, M.B.B. Pereira, L.S. Silva, E.C. Silva Filho, I.M.G. Santos, M.G. Fonseca, M. Jaber, Microwave bentonite silylation for dye removal: Influence of the solvent. *Appl. Clay Sci. 168* (2019), 478–487. https://doi.org/10.1016/j.clay.2018.11.027

[45] D. Karadag, E. Akgul, S. Tok, F. Erturk, M.A. Kaya, M. Turan, Basic and Reactive Dye Removal Using Natural and Modified Zeolites. *J. Chem. Eng. Data. 52* (2007), 2436–2441. https://doi.org/10.1021/je7003726

[46] P. Pengthamkeerati, T. Satapanajaru, O. Singchan, Sorption of reactive dye from aqueous solution on biomass fly ash. *J. Hazard. Mater. 153* (2008), 1149–1156. https://doi.org/10.1016/j.jhazmat.2007.09.074

[47] L.D.T. Prola, E. Acayanka, E.C. Lima, C.S. Umpierres, J.C.P. Vaghetti, W.O. Santos, P.T. Djifon,. Comparison of Jatropha curcas shells in natural form and treated by non-thermal plasma as biosorbents for removal of Reactive Red 120 textile dye from aqueous solution. *Ind. Crops Prod. 46* (2013), 328–340. https://doi.org/10.1016/j.indcrop.2013.02.018

[48] I. C. Pereira, K. Q. Carvalho, F. H. Passig, R. C. Ferreira, R.C.P. Rizzo-Domingues, M.I. Hoppen, F. Perretto, Thermal and thermal-acid treated sewage sludge for the removal of dye reactive Red 120: Characteristics, kinetics, isotherms, thermodynamics and response surface methodology design. *J. Environ. Chem. Eng. 6* (2018), 7233–7246. https://doi.org/10.1016/j.jece.2018.10.060

[49] A. K. Dey, A. Dey, Selection of optimal processing condition during removal of Reactive Red 195 by NaOH treated jute fibre using adsorption. *Groundw. Sustain. Dev. 12* (2021), 100522. https://doi.org/10.1016/j.gsd.2020.100522

[50] R. Sananmuang, W. Chuachuad Chaiyasith, K. Wongjan, Adsorption of Reactive Dyes Red 195, Blue 222, and Yellow 145 in Solution with Polyaniline-Chitosan Membrane Using Batch Reactor. *Key Eng. Mater. 751* (2017), 713–718. https://doi.org/10.4028/www.scientific.net/KEM.751.713

[51] E. K. Shirazi, J. W. Metzger, K. Fischer, A.H. Hassani, Simultaneous removal of a cationic and an anionic textile dye from water by a mixed sorbent of vermicompost and Persian charred dolomite. *Chemosphere 234* (2019), 618–629. https://doi.org/10.1016/j.chemosphere.2019.05.224

[52] H. E1 Fargani, R. Lakhmiri, N.A. Oukharaz, A. Albourine, M. Safi, O. Cherkaoui, Removal of Reactive Yellow 135 from Wastewaterof Textile Industry onto Chitosan Extracted by Hydrothermo-Chemical Method. *Chem. Mater. Res. 9* (2017), 21–29.

[53] H.H. Abdel Ghafar, E.K. Radwan, S.T. El-Wakeel, Removal of Hazardous Contaminants from Water by Natural and Zwitterionic Surfactant-modified Clay. *ACS Omega 5* (2020), 6834–6845.